Phase behavior of bidisperse ferrocolloids

Gabriel M. Range* and Sabine H. L. Klapp†
Stranski-Laboratorium für Physikalische und Theoretische Chemie, Sekretariat TC 7, Fakultät II für Mathematik und Naturwissenschaften, Technische Universität Berlin, Straße des 17. Juni 124, D-10623 Berlin, Germany
(Received 24 August 2004; published 15 December 2004)

The phase behavior of bidisperse ferrocolloids consisting of binary mixtures of dipolar hard spheres (DHS's) with different particle diameters and different dipole moments is investigated using density-functional theory in a modified mean-field approximation. We focus on the fluid phase regime, where we consider both isotropic and anisotropic states. Depending on the parameter Γ—measuring the asymmetry of the dipolar couplings—the systems display complex fluid-fluid phase behavior involving demixing transitions, as well as first- and second-order isotropic-to-ferromagnetic phase transitions. The topology of the resulting phase diagrams turns out to be similar to those corresponding to monodisperse DHS mixtures investigated previously by us [Phys. Rev. E **69**, 041201 (2004)]. However, additional size asymmetry has a strong impact on the relative importance of the various types of phase transitions. In particular, the demixing transition of bidisperse ferrocolloids is strongly destabilized compared to that of monodisperse DHS's in the sense that demixing critical points are significantly shifted towards lower temperatures.

DOI: 10.1103/PhysRevE.70.061407 PACS number(s): 82.70.Dd, 75.50.Mm, 64.70.−p, 64.75.+g

I. INTRODUCTION

Ferrocolloids are stable colloidal suspensions of small magnetic particles in a carrier liquid like water or oil [1]. The permanent magnetic dipole moment of the single-domain particles is proportional to the volume of their magnetic cores. In ferrocolloids, polydispersity in the particle sizes (which is an essentially omnipresent feature of colloidal systems) therefore yields automatically a nonuniformity in the distribution of magnetic moments and the resulting dipole-dipole interaction strength. The effect of this nonuniformity on material properties such as magnetization, microstructure (in particular, cluster formation), and viscosity has been intensely studied both experimentally [1] and, more recently, also by computer simulation [2–6] and theory [7]. However, most of these studies are restricted to the investigation of one or a few thermodynamic states corresponding to highly dilute ferrocolloid systems.

Less is known about the influence of polydispersity on the overall phase behavior. In a recent computer simulation study [8], Kristof *et al.* have calculated vapor-liquid coexistence curves of various polydisperse ferrocolloids at *one* (fixed) total density. The results imply saturation of larger (i.e., more strongly interacting) particles in the denser phase, indicating that vapor-liquid transitions in polydisperse ferrocolloids are to some extent coupled with *demixing* phase transitions. This is in qualitative agreement with experiments [9,10] and also with earlier theoretical studies [11,12], where—as a first approximation for polydispersity—*bidisperse* systems consisting of two fractions of magnetic particles with significant size differences have been considered. However, a broader understanding of the link between the nature and degree of nonuniformity and the macroscopic phase behavior, in particular the appearance of demixing phase transitions, is still missing.

As a contribution to fill this gap we have recently presented [13] a systematic study of the fluid-fluid phase behavior of the most simple model for a polydisperse ferrocolloid, which is a binary mixture of dipolar hard spheres (DHS's) with different dipole moments m_A and m_B but *equal* sizes. In order to elucidate the effect of additional size nonuniformity we consider in the present study an extended binary DHS model involving different diameters σ_A and σ_B, to which the dipole moments $m_A \propto \sigma_A^3$ and $m_B \propto \sigma_B^3$ are coupled as in real systems. Following our ealier work [13], we perform our investigations on the basis of density-functional theory in the so-called modified mean-field (MMF) approximation [14–16]. Despite various shortcomings [17], the great advantage of MMF theory compared to computer simulations or integral equation theories is that it allows one to scan phase diagrams for large portions of the parameter space with reasonable computational effort.

The remainder of this paper is organized as follows. In Sec. II we describe our model and summarize key expressions of MMF density-functional theory for dipolar binary mixtures [13]. Numerical results are presented in Sec. III, where we first consider mixture phase diagrams in the concentration-packing fraction plane at various temperatures. This is completed in Sec. III B 3 by a presentation of the corresponding phase diagrams in a plane spanned by the chemical potentials, which are input quantities in our theory. Finally, in order to sort out the effect of size asymmetry *on top* of dipolar interaction asymmetry we compare in Sec. III C the behavior of a specific bidisperse DHS mixture to that of the corresponding mixture monodisperse in size ($m_B < m_A, \sigma_B = \sigma_A$). Our conclusions are summarized in Sec. IV.

II. THEORY

A. Model

We consider a bidisperse ferrocolloid modeled by two species (A and B) of dipolar hard spheres with permament

*Electronic address: gabriel.range@fluids.tu-berlin.de
†Electronic address: sabine.klapp@fluids.tu-berlin.de

 ©2004 The American Physical Society

dipole moments m_A and m_B and diameters σ_A and $\sigma_B \neq \sigma_A$. The hard cores are assumed to be additive—that is,

$$\sigma_{ab} = (\sigma_a + \sigma_b)/2, \tag{2.1}$$

where the subscripts a and b denote the components considered $[a(b)=A,B]$. The magnetic dipole moments of the particles are coupled to the diameters via the relation

$$m_a = m\mathcal{V}_a, \tag{2.2}$$

where m is the specific magnetization and $\mathcal{V}_a = \pi\sigma_a^3/6$ is the volume of the particle. The resulting pair potential between two particles with coordinates $(1)=(\mathbf{r}_1,\omega_1)$ and $(2)=(\mathbf{r}_2,\omega_2)$ is given as

$$u_{ab}(12) = \begin{cases} \infty, & r_{12} < \sigma_{ab}, \\ u_{ab}^{\mathrm{dip}}(\mathbf{r}_{12},\omega_1,\omega_2), & r_{12} > \sigma_{ab}, \end{cases} \tag{2.3}$$

where $r_{12}=|\mathbf{r}_{12}|=|\mathbf{r}_2-\mathbf{r}_1|$ is the particle separation and $\omega=(\theta,\phi)$ represents the orientation of a dipole in a spatially fixed coordinate system. The dipolar potential is given by

$$\mathrm{u}_{ab}^{\mathrm{dip}}(\mathbf{r}_{12},\omega_1,\omega_2) = \frac{m_a m_b}{r_{12}^3}[\hat{\mathbf{m}}(\omega_1)\cdot\hat{\mathbf{m}}(\omega_2) - 3(\hat{\mathbf{m}}(\omega_1)\cdot\hat{\mathbf{r}}_{12}) \times(\hat{\mathbf{m}}(\omega_2)\cdot\hat{\mathbf{r}}_{12})], \tag{2.4}$$

where $\hat{\mathbf{m}}(\omega)$ and $\hat{\mathbf{r}}_{12}$ are unit vectors in the direction of ω and $\mathbf{r}_{12}$, respectively. Since we are interested in spatially homogeneous, but possibly orientationally ordered (ferromagnetic) phases, we consider fluid states with singlet densities

$$\rho_a(\mathbf{r}_1,\omega_1) = \frac{\rho_a}{2\pi}\overline{\alpha}_a(\cos\theta) = \frac{\rho_a}{2\pi}\left(\frac{1}{2} + \sum_{l=1}^{\infty}\alpha_{a,l}\mathcal{P}_l(\cos\theta)\right), \tag{2.5}$$

where $\overline{\alpha}_a(\cos\theta)$ is a normalized orientational distribution function $[\int_{-1}^{1}dx\overline{\alpha}_a(x)=1]$ and θ is the angle relative to the director of the orientational order (if present). Consequently, we can expand the distribution in Legendre polynomials $\mathcal{P}_l$ [see second member of Eq. (2.5)], where the coefficients $\alpha_{a,l}$ are connected to the usual lth-rank order paramters $P_{a,l}$ via

$$P_{a,l} = \int_{-1}^{1} dx\overline{\alpha}_a(x)\mathcal{P}_l(x) = \frac{2}{2l+1}\alpha_{a,l}. \tag{2.6}$$

The isotropic phase is specified by $P_{a,l\geq 1}=0$—i.e., $\overline{\alpha}_a(x)=1/2$—whereas a ferromagnetic phase is characterized by $P_{a,l}\neq 0$ for all l.

B. Modified mean-field density-functional theory

In order to calculate the phase behavior of the model ferrocolloids under consideration we employ density-functional theory in the modified mean-field approximation. We restrict our presentation here to the key expressions, since detailed descriptions of the MMF approach can be found in Refs. [14,15] and in Ref. [13], where we applied the same theory to DHS mixtures with *equal* diameters.

The central quantity is the grand canonical density functional Ω of the mixture

$$\frac{\Omega}{\mathcal{V}} = (F^{\mathrm{id}} + F^{\mathrm{HS}} + F^{\mathrm{dip}})/\mathcal{V} - \sum_a \mu_a\rho_a, \tag{2.7}$$

with the ideal gas part (F^{id}), the hard-sphere (HS) excess part (F^{HS}), and a part which stems from the dipolar interaction (F^{dip}). The ideal part is given by

$$\frac{F^{\mathrm{id}}}{\mathcal{V}} = \sum_a \frac{\rho_a}{\beta}[\ln(\rho_a\Lambda_a^3) - 1] + \sum_a \frac{\rho_a}{\beta}\int_{-1}^{1} dx\overline{\alpha}_a(x)\ln[2\overline{\alpha}_a(x)], \tag{2.8}$$

where $\mathcal{V}$ is the Volume, Λ_a is the thermal wavelength, and $\beta=1/k_{\mathrm{B}}T$ is the inverse temperature. The second term in Eq. (2.8) accounts for the loss of entropy in anisotropic configurations [it vanishes for $\overline{\alpha}_a(x)=1/2$].

For the hard-sphere excess part we choose the Boublik-Mansoori-Carnahan- Starling-Leland (BMCSL) approximation [18–20]

$$\frac{F^{\mathrm{HS}}}{\mathcal{V}} = \frac{\rho}{\beta}\left[\left(\frac{\xi_2^3}{\xi_0\xi_3^2} - 1\right)\ln(1-\xi_3) + \frac{3\xi_1\xi_2}{\xi_0(1-\xi_3)} + \frac{\xi_2^3}{\xi_3\xi_0(1-\xi_3)^2}\right], \tag{2.9}$$

with the total number density $\rho=\rho_A+\rho_B$ and the moments

$$\xi_i = \frac{\pi}{6}\sum_a \rho_a\sigma_a^i. \tag{2.10}$$

For the special case $\sigma_A=\sigma_B$, the BMCSL approximation reduces to the Carnahan-Starling expression for one-component HS fluids [21], which we used in our previous study of monodisperse DHS mixtures [13].

The MMF approximation enters into the dipolar contribution F^{dip}, where the pair correlation involved in the exact expression for F^{dip} is set to its low density limit—i.e., $g_{ab}(12)\to\exp[-\beta u_{ab}(12)]$. As a result, the excess free energy reduces to a quadratic form in the densities and order parameters [13],

$$\frac{F^{\mathrm{dip}}}{\mathcal{V}} = \sum_{ab}\rho_a\rho_b\sum_{l=0}^{\infty} u_{ab,l}\alpha_{a,l}\alpha_{b,l}, \tag{2.11}$$

where $\alpha_{a,0}=1/2$ and the coupling parameters are given as a power series in terms of the dipole moments—that is,

$$u_{ab,l} = \sum_{n=0}^{\infty} u_{ab,l}^{(n)}(m_a m_b)^n. \tag{2.12}$$

For $n>1$, the temperature-dependent coefficients $u_{ab,l}^{(n)}$ appearing in Eq. (2.12) are defined by

$$u_{ab,l}^{(n)} = -\frac{1}{2\beta}\frac{1}{4\pi^2 n!}(-\beta)^n\int_{\sigma_{ab}}^{\infty} dr_{12}\frac{1}{r_{12}^{3n-2}} \times\int d\omega_1 d\omega_2 d\omega_{12}\mathcal{P}_l(\cos\theta_1)\mathcal{P}_l(\cos\theta_2) \times\tilde{\Phi}_{112}^n(\omega_1,\omega_2,\omega_{12}), \tag{2.13}$$

TABLE I. The coefficients $u_{ab,l}^{(n)}$ [see Eq. (2.13)] for $l,n \leqslant 4$.

	$n=1$	$n=2$	$n=3$	$n=4$
$l=0$	0	$-\frac{8\pi}{3}\frac{\beta}{3\sigma_{ab}^3}$	0	$-\frac{8\pi}{25}\frac{\beta^3}{9\sigma_{ab}^9}$
$l=1$	$-\frac{8\pi}{27}$	0	$-\frac{16\pi}{225}\frac{\beta^2}{6\sigma_{ab}^6}$	0
$l=2$	0	$-\frac{8\pi}{375}\frac{\beta}{3\sigma_{ab}^3}$	0	$-\frac{32\pi}{6125}\frac{\beta^3}{9\sigma_{ab}^9}$
$l=3$	0	0	$\frac{16\pi}{25725}\frac{\beta^2}{6\sigma_{ab}^6}$	0
$l=4$	0	0	0	$-\frac{8\pi}{99225}\frac{\beta^3}{9\sigma_{ab}^9}$

where $\tilde{\Phi}_{112}$ describes the angle dependence of u_{ab}^{dip}—that is,

$$\tilde{\Phi}_{112}(\mathbf{r}_{12},\omega_1,\omega_2) = \{\hat{\mathbf{m}}(\omega_1)\cdot\hat{\mathbf{m}}(\omega_2) - 3[\hat{\mathbf{m}}(\omega_1)\cdot\hat{\mathbf{r}}_{12}] \times[\hat{\mathbf{m}}(\omega_2)\cdot\hat{\mathbf{r}}_{12}]\}. \tag{2.14}$$

The angular integrals in Eq. (2.13) can be solved as described in Ref. [13]. The coefficient corresponding to $n=1$ in Eq. (2.12) is related to an integral over the long-range dipolar potential itself and therefore requires special treatment (see Ref. [13] and references therein). One eventually obtains

$$u_{ab,l}^{(1)} = -\frac{8\pi}{27}\delta_{l,1}. \tag{2.15}$$

In practice, we truncate the Taylor expansion appearing in Eq. (2.12) at $n_{\max}=4$. Explicit expressions for the resulting set $(l,n\leqslant 4)$ of coefficients $u_{ab,l}^{(n)}$ [after performing the angular integrals in Eq. (2.13)] are given in Table I. In order to identify the set of ten parameters $(\{\rho_a,\alpha_{a,1},\ldots,\alpha_{a,4}\})$ characterizing the equilibrium state at a given $(\mu_a,T,\mathcal{V})$, we solve the Euler-Lagrange equations

$$\frac{\partial(\Omega/\mathcal{V})}{\partial\rho_a}=0, \quad \frac{\delta(\Omega/\mathcal{V})}{\delta\overline{\alpha}_a(x)}=0. \tag{2.16}$$

This is done numerically by employing a multidimensional Newton-Raphson algorithm.

1. Searching for coexisting states

In order to find two *coexisting* states at a given temperature T one has to search for those chemical potentials μ_A^{coex} and μ_B^{coex} where the pressures of the two states (1 and 2) considered are identical—that is

$$p_1 = -\Omega[\rho_{a,1}^{\mathrm{eq}},\overline{\alpha}_{a,1}^{\mathrm{eq}}(x)]/\mathcal{V} = p_2 = -\Omega[\rho_{a,2}^{\mathrm{eq}},\overline{\alpha}_{a,2}^{\mathrm{eq}}(x)]/\mathcal{V}. \tag{2.17}$$

In Eq. (2.17), $\rho_{a,i}^{\mathrm{eq}}$ and $\overline{\alpha}_{a,i}^{\mathrm{eq}}(x)$, $i=1,2$, are two equilibrium states satisfying Eq. (2.16). In practice, we perform the search for μ_A^{coex} and μ_B^{coex} by using the ansatz

$$(\mu_A^{\mathrm{coex}},\mu_B^{\mathrm{coex}}) = \lambda\boldsymbol{\mu} + \nu\boldsymbol{\mu}_\perp, \tag{2.18}$$

where λ and ν are coefficients, which have to be determined using Eq. (2.17), and the vectors $\boldsymbol{\mu}$ and $\boldsymbol{\mu}_\perp$ specify two orthogonal, fixed directions in the plane spanned by μ_A and μ_B. A good choice to investigate isotropic-to-ferromagnetic transitions is the directions $\boldsymbol{\mu}=(-1,1)$ and $\boldsymbol{\mu}_\perp=(1,1)$, implying that a change of λ corresponds to a variation of the chemical potential difference $\Delta\mu=\mu_B-\mu_A$, while a change of ν corresponds to a variation of the total chemical potential $\mu=\mu_A+\mu_B$. The search is started from some known initial solution (e.g., a phase coexistence of a pure A fluid) specified by the coefficients (λ_0,ν_0). Increasing λ successively from λ_0, we determine the coexistence values of ν—and therefore the pairs $(\mu_A^{\mathrm{coex}},\mu_B^{\mathrm{coex}})$—by performing an (one-dimensional) Newton-Raphson algorithm on the coefficient ν. To determine demixing transitions, which usually occur at high packing fractions, it is more appropriate to successively increase the total chemical potential, therefore setting $\boldsymbol{\mu}=(1,1)$ and $\boldsymbol{\mu}_\perp=(-1,1)$. Hence, the temperature and chemical potential difference $(T,\Delta\mu)$ are the adequate tuning parameters to explore isotropic-to-ferromagnetic coexistences, while we use

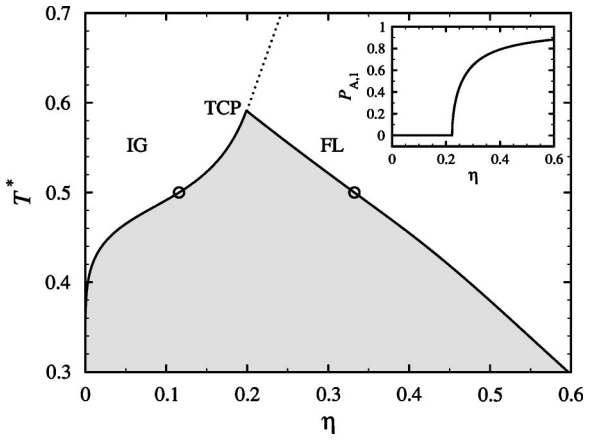

FIG. 1. MMF phase diagram of a monodisperse DHS fluid containing only A particles in the packing fraction-temperature plane $[T^*=k_BT\sigma_A^3/m_A^2, \eta=(\pi/6)\rho_A\sigma_A^3]$. The inset shows the η dependence of $P_{A,1}$ at $T^*=0.65$. For an explanation of the lines and symbols, see the main text.

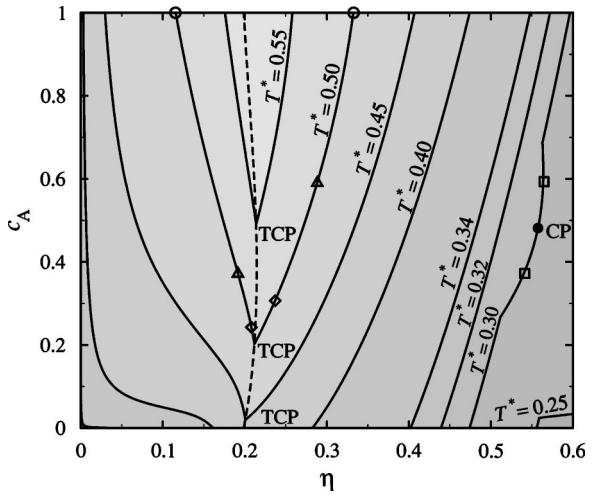

FIG. 2. Packing fraction-concentration phase diagram for a bidisperse ferrocolloid with $\Gamma=0.75$ at various temperatures. For explanation of the various lines, see the main text. The pairs of open symbols denote coexisting states at $T^*=0.50/\Delta\mu^*=-\infty$ (circles), $T^*=0.50/\Delta\mu^*=0.6$ (triangles), $T^*=0.50/\Delta\mu^*=0.9$ (diamonds), and $T^*=0.30/\mu^*=-5.5$ (squares). The solid circle denotes a demixing critical point.

the temperature and total chemical potential (T,μ) as tuning parameters to search for demixing transitions.

III. RESULTS AND DISCUSSION

A. Reduced quantities and the one-component case

In the grand-canonical ensemble the state of the mixtures can be characterized by the reduced temperature $T^*=k_BT\sigma_A^3/m_A^2$, the size ratio $s=\sigma_B/\sigma_A$, the dipolar interaction parameter $\Gamma=(m_B^2\sigma_A^3)/(m_A^2\sigma_B^3)$, the total chemical potential $\mu^*\equiv\mu_A^*+\mu_B^*$, and the chemical potential difference $\Delta\mu^*\equiv\mu_B^*-\mu_A^*$, where $\mu_a^*=\sigma_A^3/m_A^2[\mu_a-\beta^{-1}\ln(\Lambda_a^3/\sigma_A^3)]$. Minimization of the density functional then yields, along with the orientational order parameters, the reduced densities $\rho_a^*=\rho_a\sigma^3$. Instead of these latter quantities, we employ here the packing fraction $\eta=(\pi/6)\Sigma_a\sigma_a^3\rho_a$ and the concentration $c_A=\sigma_A^3\rho_A/(\Sigma_a\sigma_a^3\rho_a)$ of species A as density order parameters.

In the limit $\Delta\mu^*\to-\infty$ one recovers the MMF phase diagram of a one-component DHS fluid containing only species A (i.e., $c_A=1$). Results in the η-T^* plane are shown in Fig. 1. Disregarding any solid structures (which are not captured by the present approach) there are two phases involved: an isotropic gas (IG) with zero orientational order parameters (i.e., $P_{A,l\geqslant1}=0$) appearing at low and intermediate packing fractions and a ferromagnetic liquid (FL) with $P_{A,l\geqslant1}>0$ appearing at higher packing fractions (see the inset in Fig. 1). Below the temperature $T^*_{\mathrm{TCP}_A}$ related to the *tricritical point* (TCP) of the A fluid the transition between the two phases is of first order both in η and in the orientational order parameters $P_{A,l>1}$. An exemplary (IG)-(FL) coexistence ($T^*=0.5$) is denoted by the open circles in Fig. 1. Above $T^*_{\mathrm{TCP}_A}$ the (IG)-(FL) transition becomes continuous (see the inset in Fig. 1). The resulting *critical line* separating the isotropic and ferromagnetic phase can be found from a Landau analyis as described in Refs. [13,14].

B. Bidisperse ferrocolloids

We now turn to true *mixtures* of bidisperse ferrocolloids characterized by $s\neq1$ and finite values of the chemical potential difference $\Delta\mu^*$. The phase behavior of these systems strongly depends on the actual value of the dipolar interaction parameter Γ. The latter is coupled to the size ratio through Eq. (2.2), which implies $\Gamma=s^3$. In the following two sections we discuss characteristic phase properties at four typical values of Γ in the range $0\leqslant\Gamma\leqslant1$ (the behavior at $\Gamma\geqslant1$ then simply follows from interchanging A and B). To illustrate our results we mainly employ a "quasi-three-dimensional" representation where the phase transition lines for various temperatures are plotted in the η-c_A plane. Moreover, we present in Sec. III B 3 additional diagrams using a plane spanned by the chemical potentials—i.e., the input parameters of our theory. This additional representation not only helps to elucidate the effect of varying Γ (or s, respectively) on the mixture's phase behavior, but also to later compare (in Sec. III C) the bidisperse systems to monodisperse DHS mixtures.

1. Weakly asymmetric systems

We start by considering weakly asymmetric mixtures. A typical example is a system characterized by $\Gamma=0.75$, which corresponds to a size ratio $s\simeq0.91$. Figure 2 shows the associated phase diagram in the η-c_A plane at several temperatures T^*. In this representation, the pure A fluid discussed in Fig. 1 corresponds to the limiting case $c_A=1$ ($\Delta\mu^*\to-\infty$)—that is, the upper border of the phase diagram—while the lower border ($c_A=0$) corresponds to a pure B fluid ($\Delta\mu^*\to+\infty$). In order to understand the mixture's behavior in between these cases we first consider the dashed line in Fig. 2, which connects the tricritical points at intermediate values of the chemical potential difference. As in the one-component fluid [14], the behavior of the mixture order parameters η and c_A upon approaching a TCP (at fixed μ^*, $\Delta\mu^*$, or T^*) is characterized by the mean-field exponent β

TABLE II. Order parameters of the coexisting states in Fig. 2. Not shown are the values of $P_{a,l>2}$.

		η	c_A	$P_{A,1}$	$P_{B,1}$	$P_{A,2}$	$P_{B,2}$
Circles	IG	0.115	1.0	0.0	0.0	0.0	0.0
	FL	0.333	1.0	0.842	0.768	0.604	0.473
Triangles	IG	0.192	0.372	0.0	0.0	0.0	0.0
	FL	0.288	0.590	0.772	0.676	0.479	0.345
Diamonds	IG	0.208	0.243	0.0	0.0	0.0	0.0
	FL	0.237	0.307	0.570	0.454	0.232	0.142
Squares	FL_A	0.565	0.593	0.971	0.954	0.916	0.870
	FL_B	0.541	0.372	0.968	0.950	0.908	0.859

$=1$. In Fig. 2, the crossing of the line of TCP's with the upper (lower) horizontal at $c_A=1$ (0) indicates the packing fraction corresponding to the TCP's of the pure fluids—that is, $\eta_{\mathrm{TCP}_A}=\eta_{\mathrm{TCP}_B}$. Also, states on the left- (right-) hand side of the line of TCP's are isotropic (ferromagnetic). The shape of the dashed line then implies that, upon increasing $\Delta\mu^*$ from $-\infty$ to $+\infty$, the concentration c_A of the TCP decreases monotonically to zero, while the packing fraction remains essentially constant. At the same time the temperatures T^*_{TCP} decrease monotonically from $T^*_{\mathrm{TCP}_A}\simeq 0.59$ to $T^*_{\mathrm{TCP}_B}=\Gamma T^*_{\mathrm{TCP}_A}\simeq 0.44$ (where the latter relation follows from our definition of T^* and Γ). This indicates that the isotropic-ferromagnetic transition in the mixture is generally *destabilized* compared to the one-component case (i.e., the pure A fluid). This destabilization is not a simple scaling effect (resulting from the different dipole moments) in the sense that the tricritical temperatures do not depend linearly (only monotonically) on the concentration of the weaker species.

Further information is gained from the two-phase coexistence lines, which are indicated by the solid lines in Fig. 2. Also, the symbols denote exemplary coexisting states, the order parameters of which are given in Table. II. For orientation consider first the pair of open circles at the upper border ($c_A=1$) of the diagram, which denotes an (IG)-(FL) phase coexistence of the pure A fluid at temperature $T^*=0.5$ (see the corresponding pair of open circles in Fig. 1). Starting from these states and increasing $\Delta\mu^*$ (with the temperature kept fixed), the (IG)-(FL) phase coexistence remains at first, but the two coexisting states develop a difference in the concentration c_A. This is illustrated by the relative location of the two triangles in Fig. 2 and the corresponding values of c_A in Table II, from which it follows that the ferromagnetic phase is more saturated in A than the coexisting isotropic phase. We understand this preference as a consequence of the (relative to the B component) stronger coupling between A particles, which—in combination with the higher packing fraction—leads to a stronger mean field for A particles. For the same reason the A particles are also stronger oriented—i.e., $P_{A,l}>P_{B,l}$. Increasing $\Delta\mu^*$ even further the (IG)-(FL) coexistence finally terminates into a TCP, where the $P_{a,l\geqslant 1}$ of the ferromagnetic phase vanish. Similar phase behavior is found at other temperatures in the range $T^*_{\mathrm{TCP}_B}\leqslant T^*\leqslant T^*_{\mathrm{TCP}_A}$, and we conclude that the general mixture phase behavior in this temperature range is essentially just an

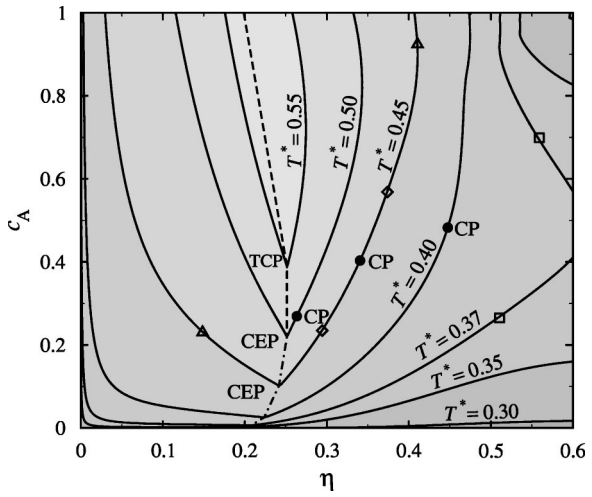

FIG. 3. Same as Fig. 2, but for $\Gamma=0.60$. The pairs of open symbols denote coexisting states at $T^*=0.45/\Delta\mu^*=1.0$ (triangles), $T^*=0.45/\Delta\mu^*=1.42$ (diamonds), and $T^*=0.37/\mu^*=4.0$ (squares).

"interpolation" between the (IG)-(FL) coexistence of the pure A and that of the pure B fluid.

Only at substantially lower temperatures does one encounter new phase behavior characterized by the appearance of additional critical points (CP's) deep within the ferromagnetic regime (see Fig. 2). Approaching these CP's from low temperatures (at fixed μ^* or $\Delta\mu^*$) the differences between the order parameters of the two coexisting phases vanish with the (mean-field) exponent $\beta=1/2$. An exemplary coexisting state is indicated by the pair of squares ($T^*=0.3$, $\mu^*=-5.5$), and the corresponding order parameters are given in Table II. It is seen that the two coexisting phases differ mainly in c_A, while the corresponding values of η and $P_{a,l}$ are very close. One thus concludes that the additional critical points are essentially due to *demixing* phase transitions, a genuine mixture phenomenon which is clearly absent in pure fluids. We note, however, that demixing appearently only comes into play at very high values of η—in fact, at packing fractions outside the fluid phase regime. As a consequence, the line of tricritical points, which are characterized by significantly smaller packing fractions than those associated with the demixing CP, remains essentially unaffected by demixing.

2. Moderate and strongly asymmetric mixtures

Decreasing the size ratio, and thereby Γ, from the value discussed in Sec. III B 1 one generates mixtures with more asymmetric dipolar interactions. Figure 3 illustrates the phase behavior at $\Gamma=0.60$ ($s\simeq 0.84$). At this degree of asymmetry, the topology of the phase diagram is essentially still the same as at $\Gamma=0.75$. However, closer inspection reveals that the temperatures related to the demixing CP's are substantially larger than at $\Gamma=0.75$, while the packing fractions characterizing the demixed states are much smaller. These changes reflect the increased tendency of the more asymmetric system to demix. In fact, for temperatures $T^*\lesssim 0.50$ the demixing tendency "interferes" so strongly with the tricriti-

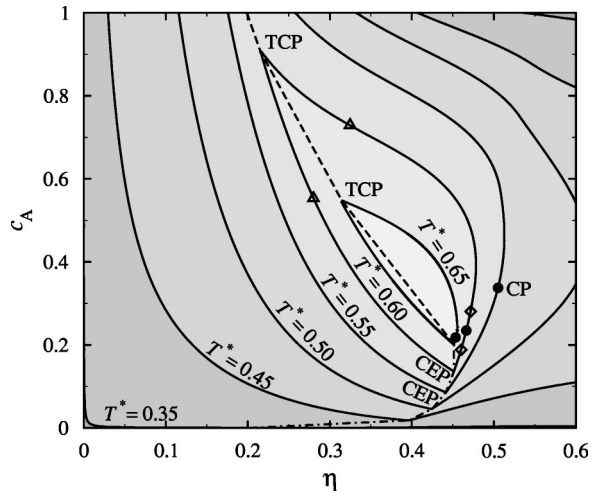

FIG. 4. Same as Fig. 2, but for $\Gamma=0.40$. The pairs of open symbols denote coexisting states at $T^*=0.60/\mu^*=3.0$ (triangles) and $T^*=0.60/\mu^*=17.9$ (diamonds).

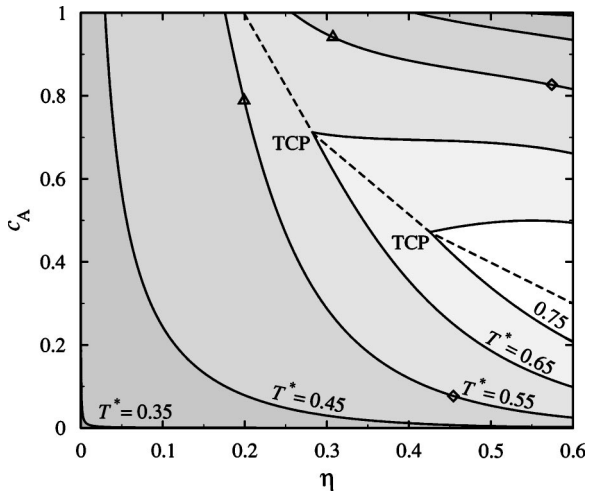

FIG. 5. Same as Fig. 2, but for $\Gamma=0.30$. The pairs of open symbols denote coexisting states at $T^*=0.55/\mu^*=0.0$ (triangles) and $T^*=0.55/\mu^*=20.0$ (diamonds).

cal line that the TCP is replaced by a *critical end point* (CEP). Its meaning is illustrated by the exemplary coexisting states indicated on the $T^*=0.45$ line in Fig. 3: Upon increasing $\Delta\mu^*$ from strongly negative values (pure A fluid), the two-phase (IG)-(FL) coexistence does not terminate at some critical value $\Delta\mu^*_{\mathrm{TCP}}$. Instead, the (IG)-(FL) coexistence changes continuously into a (FL_B)-(FL_A) coexistence and finally terminates into a demixing CP. The "perturbation" of the (IG)-(FL) transition by demixing transitions becomes even more pronounced upon further decrease of Γ. An example is shown in Fig. 4 where the phase diagram is plotted for $\Gamma=0.40$ ($s\simeq 0.74$). Most significant here is the appearance of *closed* coexistence loops at temperatures larger than $T^*_{\mathrm{TCP}_A}\simeq 0.59$. To understand their meaning we consider the exemplary temperature $T^*=0.6$. Starting from the pure A fluid, which displays a second-order (IG)-(FL) transition, and increasing μ^*, one observes at first the appearance of a TCP. Further increase of the chemical potential results in a (IG)-(FL) phase coexistence (see pair of triangles in Fig. 4), which implies that the TCP must have moved towards higher temperatures. After a transformation TCP$\rightarrow$CEP, the (IG)-(FL) coexistence then changes into a (FL_B)-(FL_A) coexistence, as indicated by the pair of diamonds in Fig. 4. Upon further increase of μ^* the coexistence region finally closes at the demixing critical point. The appearance of loops in the packing fraction-concentration diagrams thus reflects the *nonmonotonic* behavior of T^*_{TCP} upon varying μ^*, which is in contrast to the mononotic behavior observed in more symmetric mixtures (see Sec. III B 1). A further difference appears when one compares the locations of the TCP's and CEP's at intermediate temperatures such as $T^*=0.5$ or $T^*=0.45$, for example. It is seen that the TCP's and CEP's become related to significantly higher packing fractions, indicating a *destabilization* of the isotropic-ferromagnetic transition. Finally, when turning to even more asymmetric mixtures such as $\Gamma=0.30$ ($s\simeq 0.67$) (cf. Fig. 5), the phase diagram becomes completely dominated by demixing transitions.

3. Phase diagrams in the chemical potential plane

It is instructive to view the results from Secs. III B 1 and III B 2 also in the plane spanned by the thermodynamic input parameters $\mu^*=\mu^*_A+\mu^*_B$ and $\Delta\mu^*=\mu^*_B-\mu^*_A$.

The resulting μ^*-$\Delta\mu^*$ phase diagrams for the four values of Γ under investigation are displayed in Figs. 6(a)–6(d). Within our definition of reduced parameters, the behavior of the pure $A(B)$ fluid is recovered in the limits $\Delta\mu^*\rightarrow-\infty(+\infty)$ and $\mu^*\rightarrow-\infty$. Therefore, the solid lines at small μ^*, which approach the slope $\mathrm{d}\Delta\mu^*/\mathrm{d}\mu^*=+1[-1]$, correspond to the (IG)-(FL_A) [(IG)-(FL_B)] coexistences of the pure systems. At temperatures larger than $T^*_{\mathrm{TCP}_A}$ [$T^*_{\mathrm{TCP}_B}$], these solid lines are replaced by dashed lines corresponding to the second-order (IG)-(FL_A) [(IG)-(FL_B)] transitions of the pure systems. On the other hand, the (FL_A)-(FL_B) coexistences resulting from demixing transitions in dense mixtures (see Sec. III B 2) are indicated in Figs. 6(a)–6(d) by the solid lines appearing at larger μ^*. A crossing of three solid lines then indicates a triple point (IG)-(FL_A)-(FL_B).

Given these implications, the μ^*-$\Delta\mu^*$ phase diagram at $\Gamma=0.75$ [see Fig. 6(a)] reveals that the high-temperature behavior of this mixture is essentially an interpolation of pure A and B fluids. Demixing transitions at this degree of asymmetry only come into play at very low temperatures, in accordance to our discussion in Sec. III B 1. The representation in Fig. 6(a) additionally shows that these low-temperature (FL_A)-(FL_B) coexistences occur at positive values of $\Delta\mu^*$, indicating that the presence of B particles has to be favored (relative to that of A particles) in order to realize demixing phase transitions. We understand this as a consequence of the fact that the B particles are coupled less strongly than the A particles. Therefore, only a strong perturbation of the A fluid by B particles yields demixing. Less obvious is why the values of $\Delta\mu^*$ associated with the (FL_A)-(FL_B) coexistence apparently *decrease* with increasing μ^*. In this context it is worth remembering that $\Delta\mu^*$ is a quantity describing which species (A or B) can be inserted into the system with lower

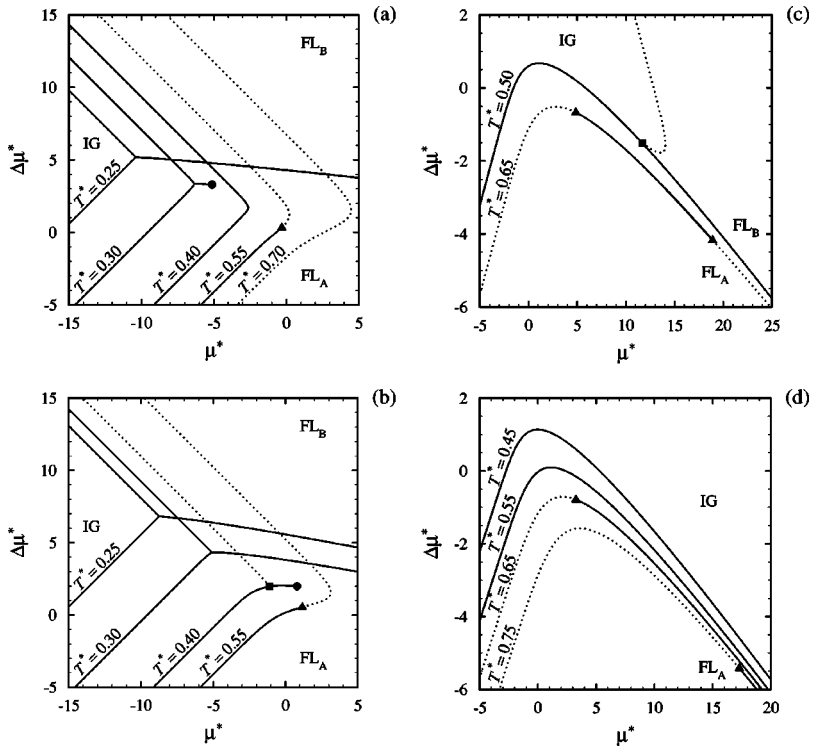

FIG. 6. μ^*-$\Delta\mu^*$ phase diagrams for bidisperse ferrocolloid with (a) $\Gamma=0.75$, (b) $\Gamma=0.60$, (c) $\Gamma=0.40$, and (d) $\Gamma=0.30$, at different temperatures T^*. Solid (dotted) lines denote two-phase coexistence (critical) lines. Solid circles, triangles, and squares denote CP's, TCP's, and CEP's, respectively.

energetic effort. Given this definition, we interpret the decrease of $\Delta\mu^*$ such that the higher the packing fraction becomes, the more and more it gets difficult to insert *A* particles. This is a direct consequence of the bidisperse nature of the underlying HS system, where it is easier to insert small particles (*B*) than large ones (*A*). Clearly this effect gets even more pronounced for more strongly differing particle sizes [see Figs. 6(b)–6(d)]. Indeed, as we will later see, the decrease of $\Delta\mu^*$ with μ^* is one of the specific features of bidisperse ferrocolloids relative to monodisperse systems with asymmetric dipolar interactions.

Compared to the case $\Gamma=0.75$, the new feature of the phase diagram at $\Gamma=0.60$ [see Fig. 6(b)] is (apart from quantitative differences already discussed in Sec. III B 2) the appearance of a CEP at temperatures in between $T^*_{\mathrm{TCP}_A}$ and $T^*_{\mathrm{TCP}_B}$. This phenomenon reflects the increasing importance of demixing transitions relative to the (IG)-(FL) transitions occurring already in the pure fluids. The topology of the μ^*-$\Delta\mu^*$ phase diagram changes even more upon further reduction of Γ [see Figs. 6(c) and 6(d)]. An important feature is the appearance of "islands" of first-order transitions in between second-order transitions at $\Gamma=0.40$ and temperatures *larger* than $T^*_{\mathrm{TCP}_A}$ [see, for example, $T^*=0.65$ in Fig. 6(c)]. Furthermore, as seen both at $\Gamma=0.40$ and at $\Gamma=0.30$, the demixing transitions become shifted not only towards higher and higher temperatures, but also towards more and more *negative* values of $\Delta\mu^*$ due to the smaller size ratio *s*.

C. Ferrocolloids compared to monodisperse DHS mixtures

In view of the rich phase behavior observed for our ferrocolloid mixtures one may ask whether this behavior results primarily from the asymmetric dipolar couplings—that is, the different dipole moments—or rather from the *combination* of different dipole moments and different sizes of the dipolar spheres. It is therefore instructive to compare the results of the present study with previous work by us [13], where we employed MMF theory in order to investigate binary DHS mixtures with different dipole moments m_A and m_B, but *equal* diameters $\sigma=\sigma_A=\sigma_B$. As an example, we compare in Fig. 7 the η-c_A phase diagrams of monodisperse and bidisperse systems at $\Gamma=0.4$ (i.e., both systems have the same dipolar coupling strength). Clearly, the phase diagrams are similar from a topological point of view. Specifically, both diagrams contain features such a CEP's and demixing CP's, as well as "islands" of coexistence at temperatures $T^*>T^*_{\mathrm{TCP}_A}$. Similar agreement is found at other values of the interaction ratio, indicating that size asymmetry on top of the dipolar asymmetry has little impact. To illustrate these more subtle changes we compare in Fig. 8 the μ^*-$\Delta\mu^*$ phase diagrams corresponding to the η-c_A diagrams in Fig. 7 at the exemplary temperature $T^*=0.5$. One finds that pronounced differences between the two systems only occur at large μ^* and intermediate values of $\Delta\mu^*$—that is, in the parameter range corresponding to the demixing transitions. This becomes understandable when one takes into account that demixing transitions are associated with relatively high packing fractions (see Fig. 7). Under these conditions, the free energy of the dipolar mixtures will be dominated by the contribution F^{HS} [see Eq. (2.9)] stemming from the underlying HS systems. The latter contribution, however, will strongly depend on whether one considers the bidisperse or monodisperse case. In dense and strongly asymmetric bidisperse mixtures it

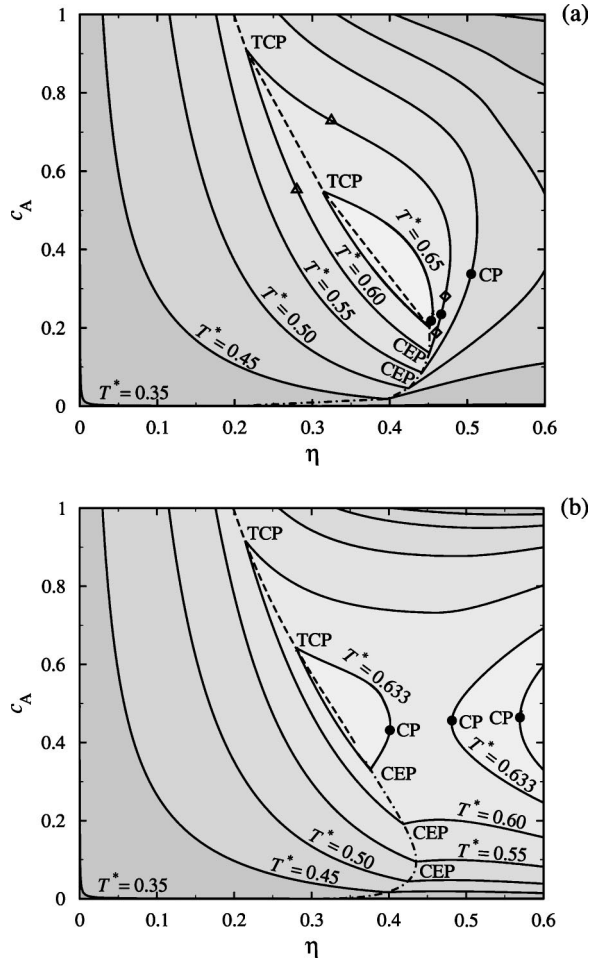

FIG. 7. (a) Same as Fig. 4 and (b) η-c_A phase diagram of a monodisperse DHS mixture at $\Gamma=0.4$ [13].

is entropically favorable to insert small particles (B) into the mixture, yielding small values of $\Delta\mu^*$ as discussed in Sec. III B 3. In monodisperse mixtures, on the other hand, these (size-induced) entropic differences vanish, and the more

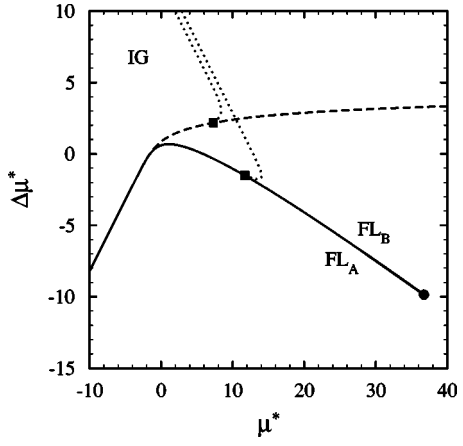

FIG. 8. Comparison of the μ^*-$\Delta\mu^*$ phase diagrams of a bidisperse ferrocolloid (solid line) and a monodisperse DHS mixture (dashed line) at $\Gamma=0.4$ and $T^*=0.5$. The solid circle denotes a CP and the solid squares denote CEP's.

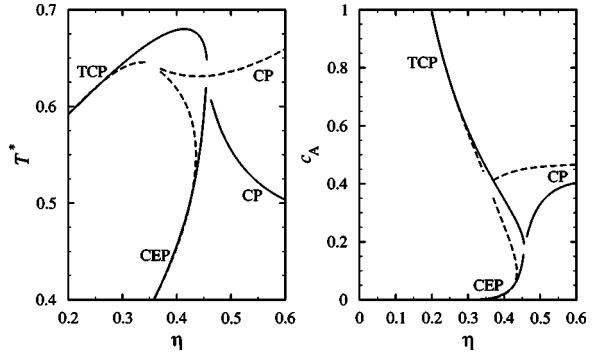

FIG. 9. Temperatures T^* (left) and concentrations c_A (right) related to the TCP's, CEP's, and CP's as functions of the packing fraction for a bidisperse ferrocolloid (solid lines) and a monodisperse DHS mixture (dashed lines) at $\Gamma=0.4$.

strongly coupled A particles can be inserted with less energetic effort (i.e., large $\Delta\mu^*$), regardless of the packing fraction. Together these effects shift the line of demixing transitions occurring in the bidisperse system towards significantly smaller values of $\Delta\mu^*$ compared to the monodisperse case, which is exactly what one sees to be the case in Fig. 8.

Further information on how bidispersity affects dipolar mixtures relative to monodisperse systems is gained from the two parts of Fig. 9 where we compare the η dependence of the temperatures and concentrations related to the (tri) critical and critical end points (again at $\Gamma=0.4$). As expected from our discussion above, results for monodisperse and bidisperse systems nearly coincide for small packing fractions, but differ for larger values of η. The most prominent difference concerns the temperatures related to the demixing CP's (see the left-hand side of Fig. 9): the CP's for monodisperse systems appear at significantly larger temperatures than for the bidisperse systems, indicating a *destabilization* of demixing with respect to the temperature range. On the other hand, the composition of bidisperse systems at the onset of demixing (i.e., at the CP's) is more dominated by B particles.

IV. CONCLUSIONS

In this work we have employed density-functional theory in the modified mean-field approximation in order to explore the fluid-fluid phase behavior of a bidisperse ferrocolloid, modeled by a binary mixture of dipolar hard spheres with different sizes σ_a and different dipole moments $m_a \propto \sigma_a^3$. Results have been obtained for four exemplary values of the parameter $\Gamma=(m_B^2\sigma_A^3)/(m_A^2\sigma_B^3)$ measuring the degree of asymmetry of the dipolar interactions within the mixture. The corresponding phase behavior turns out to be significantly richer than that of one-component DHS fluids, but at the same time quite similar to that of binary DHS fluids with different dipole moment and *equal* sizes, a system we have recently investigated using the same theoretical approach [13].

To begin with, a common feature of monodisperse and bidisperse DHS mixtures is the *destabilization* of the isotropic-to-ferromagnetic transition compared to the one-component case (i.e., the pure A fluid). Furthermore, within

the ferromagnetic phases both types of mixtures exhibit *demixing* phase transitions into *A*-rich and *B*-rich phases as soon as Γ departs from unity. For weakly asymmetric systems (i.e., Γ close to 1) these transitions occur only at very low temperatures and extremely large packing fractions. In fact, assuming that the freezing densities of our mixtures (where the size differences are relatively small) are roughly given by that of a pure HS fluid ($\eta \simeq 0.5$), it seems likely that the demixing CP in these weakly asymmetric systems will be preempted by freezing into some solid structure. We have shown, however, that demixing becomes significantly stabilized both in terms of temperature and in terms of packing fraction upon increasing the degree of asymmetry (decreasing Γ). At least for highly asymmetric systems, one may therefore expect that demixing into two fluid phases will persist even when freezing is taken into account in the theory (e.g., by following previous studies on freezing of one-component dipolar fluids [22,23]).

The already mentioned similarity between monodisperse and bidisperse DHS mixtures goes so far that the *topology* of the phase diagrams at the values of Γ considered is essentially the same. Furthermore, even on a quantitative level significant differences only appear at large total densities, with the consequence that bidispersity affects the location of the demixing rather than that of isotropic-to-ferromagnetic phase transitions. A main effect at these (large) packing fractions is that the demixing transition in the bidisperse system is shifted towards lower temperatures compared to the monodisperse case, indicating a *destabilization* of demixing. Apart from these effects, the major conclusion emerging from our study is that the role of size asymmetry on top of (dipolar) interaction asymmetry is rather unimportant for packing fractions within the fluid phase regime. Interestingly, this is consistent with observations that were recently made in a study of the phase behavior of polydisperse Lennard-Jones mixtures [24].

Given the approximate nature of the MMF theory, it is clear that comparison with results from more sophisticated approaches such as computer simulations or integral equation theories would be highly desirable. Such results are not available at the moment, but based on our previous study on equisized DHS mixtures [17], where we compared MMF results to those from reference hypernetted chain (RHNC) integral equation theory and based on the similarity between monodisperse and bidisperse mixtures observed in the present work, we can foresee some general trends. To start with, we would expect that the observed destabilization of the isotropic-to-ferromagntic transition is correct, but that the ferromagnetic transition temperatures are strongly overestimated by the MMF approach. We would also expect that bidisperse DHS mixtures (as do monodisperse mixtures) exhibit demixing already in the *isotropic* phase, which is just not reproduced within the MMF approach (where demixing appears only in the ferromagnetic phase) due to its strong overestimation of ordering tendencies. Nevertheless, given that both the MMF and RHNC approaches treat the hard-sphere part of the free energy by means of very accurate approximations [18,19,25,26], we would expect differing HS sizes to have a comparable influence in both theories and also future simulations.

ACKNOWLEDGMENT

S.H.L.K. acknowledges financial support from the Deutsche Forschungsgemeinschaft through the Emmy-Noether Program.

[1] *Ferrofluids, Magnetically Controllable Fluids and their Applications*, edited by S. Odenbach, Lecture Notes in Physics Vol. 594 (Springer-Verlag, Berlin, 2002).
[2] A. Bradbury, S. Menear, and R. W. Chantrell, J. Magn. Magn. Mater. **54**, 745 (1986).
[3] B. J. Costa Cabral, J. Chem. Phys. **112**, 4351 (2000).
[4] Z. Wang and C. Holm, Phys. Rev. E **68**, 041401 (2003).
[5] T. Kristøf and I. Szalai, Phys. Rev. E **68**, 041109 (2003).
[6] T. Kruse, A. Spanoudaki, and R. Pelster, Phys. Rev. B **68**, 054208 (2003).
[7] B. Huke and M. Lücke, Phys. Rev. E **67**, 051403 (2003).
[8] T. Kristøf, J. Liszi, and I. Szalai, Phys. Rev. E **69**, 062106 (2004).
[9] R. Massart, E. Dubois, V. Cabuil, and E. Hasmonay, J. Magn. Magn. Mater. **149**, 1 (1995).
[10] J. C. Bacri, R. Perzynski, D. Salin, V. Cabuil, and R. Massart, J. Magn. Magn. Mater. **85**, 27 (1990).
[11] A. O. Ivanov, J. Magn. Magn. Mater. **154**, 66 (1996).
[12] V. Russier, J. Colloid Interface Sci. **174**, 166 (1995).
[13] G. M. Range and S. H. L. Klapp, Phys. Rev. E **69**, 041201 (2004).
[14] B. Groh and S. Dietrich, Phys. Rev. E **50**, 3814 (1994).
[15] B. Groh and S. Dietrich, Phys. Rev. Lett. **72**, 2422 (1994).
[16] E. Lomba, J.-J. Weis, N. G. Almarza, F. Bresme, and G. Stell, Phys. Rev. E **49**, 5169 (1994).
[17] G. M. Range and S. H. L. Klapp, Phys. Rev. E **70**, 031201 (2004).
[18] T. Boublik, J. Chem. Phys. **53**, 471 (1970).
[19] G. A. Mansoori, N. F. Carnahan, K. E. Starling, and T. W. Leland, J. Chem. Phys. **77**, 3714 (1982).
[20] J. J. Salacuse and G. Stell, J. Chem. Phys. **77**, 3714 (1982).
[21] N. F. Carnahan and K. E. Starling, J. Chem. Phys. **51**, 635 (1969).
[22] B. Groh and S. Dietrich, Phys. Rev. E **54**, 1687 (1996).
[23] S. Klapp and F. Forstmann, Europhys. Lett. **38**, 663 (1997).
[24] L. Bellier-Castella, H. Xu, and M. Baus, J. Chem. Phys. **113**, 8337 (2000).
[25] E. W. Grundke and D. Henderson, Mol. Phys. **24**, 269 (1972).
[26] L. L. Lee and D. Levesque, Mol. Phys. **26**, 1351 (1973).